ICAS 2016
30th Congress of the International Council of the Aeronautical Sciences
DCC, Daejeon, Korea ; September 25-30, 2016

Numerical Simulation of RCS for A Spherical Convergent Flap Nozzle with A Non-rectangular Divergent Duct

CUI Jinhui[a], SHANG Shoutang[a], YANG Qingzhen[b], CHEN Lihai[b]

[a] *AVIC Shenyang Engine Design and Research Institute, Shenyang 110015, China*

[b] *School of Power and Energy, Northwestern Polytechnical University, Xi'an 710072, China*

Abstract: Spherical convergent flap nozzle (SCFN) is a multifunction two-dimensional thrust vector nozzle, which has pitch, yaw and reverse thrust-vectoring performance. It is being researched widely and receives much recognition. The aero-engine nozzle is the main electromagnetic scattering source of the aircraft, therefore it is of great significance to suppress and weaken electromagnetic signature of the nozzle to improve the aircraft stealth performance and existence capability. Considering security performance of fighters with SCFN, it is important to study and improve stealth performance of the SCFN. Combining iterative physical optic (IPO) method with equivalent edge currents (EEC) method, a program for calculating radar scattering characteristics of the nozzle is developed in this paper. The reliability and accuracy of the program is validated by calculating a reference model. Numerical simulation of radar cross section (RCS) using the self-developed program for three spherical convergent flap nozzles with hexagonal, bowtie and baseline rectangular divergent duct is performed during the azimuth angles from 0 degree to 40 degree. The hexagonal and bowtie divergent ducts have trailing edges with shaping measures, and the baseline rectangular divergent duct has trailing edges with no shaping measures. The results show that non-rectangular divergent duct with shaping measures can decrease the RCS greatly. Under horizontal and vertical polarizations, average edge diffraction RCS of the hexagonal and bowtie SCFN is about 20dB and 33dB lower than RCS of the baseline nozzle respectively. Considering aspects of cavity scattering, the bowtie SCFN has the best RCS characteristics. At most azimuth angles, about from 0 degree to 19 degree and from 29 degree to 40 degree, RCS of bowtie SCFN is less than RCS of hexagonal and baseline SCFN. The study results in this paper can provide theory guidance for aerospace engineering of our country. The program developed also has great application value, and can be used to calculate many other nozzles.

Key words: iterative physical optic (IPO); equivalent edge currents (EEC); radar cross section (RCS); spherical convergent flap nozzle (SCFN);

1. Introduction

Stealth performance is the main characteristic and development trend of future advanced fighters. With the development of radar detection technology, requirement of electromagnetic stealth performance has become higher and higher. Cavities such as nozzles and inlets are common in the aircraft, and can be strong scattering echo source when incident electromagnetic wave reflects many times between the inner surfaces. The aero-engine nozzle, as a kind of electrically large complex cavity, is a strong scattering echo source in the aircraft and its RCS accounts for a large proportion of aircraft RCS. Therefore, carrying out investigation about electromagnetic signature suppression measures for nozzles is of great importance to improve aircraft stealth performance.

The spherical convergent flap nozzle has been identified as having several desirable characteristics [1]. SCFN is a multifunction two-dimensional convergent-divergent thrust vector nozzle and can provide pitch, yaw and reverse thrust-vectoring capability. The advantages of SCFN also include other satisfying aspects, for example, having a reduced level of radar observables and ideal stealth performance [2-3]. SCFN can improve aircraft performance greatly, and many countries have focused on

pertinent research. According to designing experience, non-rectangular divergent duct features can provide a reduced level of observability. The current investigation mainly focuses on RCS calculation of two SCFN with hexagonal and bowtie divergent duct respectively. Both nozzles have trailing edges with shaping measures. Some researches have been carried out to analyze the aerodynamics and infrared radiation about SCFN with non-rectangular divergent duct, but researches on RCS calculation are few in our country.

IPO is a high-frequency asymptotic method to analyze scattering characteristics of electrically large cavities. This method can simulate multiple reflections of electromagnetic wave and can be programmed easily. EEC is a general method to calculate edge diffraction field and has high efficiency in calculation. It is presented in this paper that a program with above two methods is self-developed to simulate radar scattering characteristics of the nozzles.

2. Geometry Model

The nozzle model is a spherical convergent flap nozzle. It consists of a circular entrance station, a spherical convergent duct, and a hexagonal or bowtie cross-section shape of the divergent duct, as well as scarfed trailing edges [3]. Fig.1 and Fig.2 show the model configurations. Fig.3 and Fig.4 present the cross-section shape of the divergent duct.

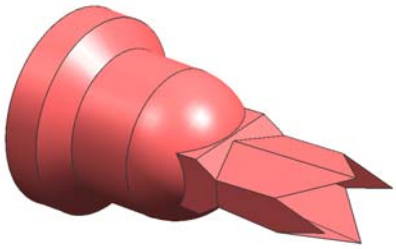

Fig.1 Configuration of SCFN with hexagonal divergent duct

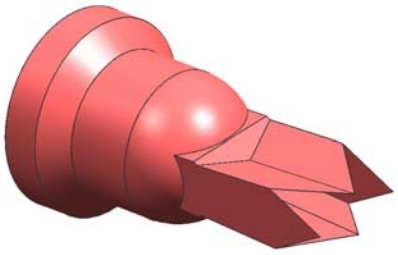

Fig.2 Configuration of SCFN with bowtie divergent duct

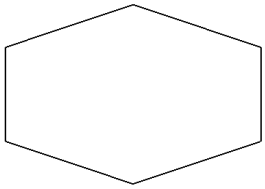

Fig.3 Cross-section of hexagonal divergent duct

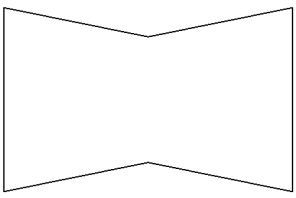

Fig.4 Cross-section of bowtie divergent duct

To demonstrate the influence of the divergent duct cross-section shape on the RCS characteristics, a baseline model with a rectangular divergent duct is investigated at the same time. Fig.5 shows the baseline model.

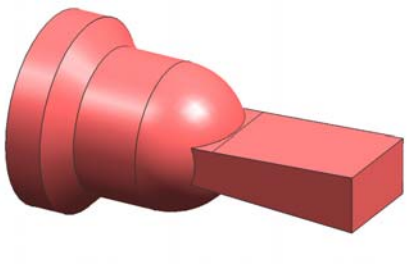

Fig.5 Configuration of the baseline SCFN

3. Iterative Physical Optic Method

The electromagnetic wave incident from the outlet of the nozzle hardly radiates out through the inlet of the aircraft, because of the existence of the complex structures, such as the turbine and combustor. Therefore the nozzle can be treated as an Open-ended cavity and the inlet of the nozzle can be simplified as a plane.

IPO proposed by F. Obelleiro etc. is an iterative method based on the physical optic approach which can simulate the multiple reflections of the electromagnetic wave in the Open-ended cavity [4]. With this method, the real electric current on the surface of the conductor is approached by the superposition of the optical current and correction current, and then the electromagnetic scattering characteristics can be obtained.

The distance between the target and the radar is so far that the incident electromagnetic wave can be treated as uniform plane wave. The electromagnetic wave incidents into an Open-ended cavity presented in Fig.6 and the initial electric current $\vec{J}_0(\vec{r}_c)$ can be obtained by physical optic approach.

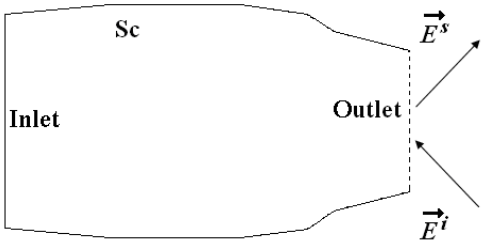

Fig.6 Sketch of an Open-ended cavity

$$\vec{J}_0(\vec{r}_c)=\begin{cases}2\vec{n}\times\vec{H}_c^i(\vec{r}_c) & \textit{lit region}\\ 0 & \textit{shadow region}\end{cases} \tag{1}$$

where $\vec{n}$ is the unit surface normal vector pointing into the cavity. $\vec{r}_c$ is the position vector of a certain point on the inner surface *Sc*. $\vec{H}_c^i(\vec{r}_c)$ denotes the incident magnetic field. The real electric current of the inner surface of the cavity can be obtained by the iterative calculation of magnetic field integral equation (MFIE).

$$\vec{J}_n(\vec{r}_c)=\vec{J}_0(\vec{r}_c)+2\vec{n}\times PV.\int_{Sc}\vec{J}_{n-1}(\vec{r}_c)\times\nabla G\left(\vec{r}_c-\vec{r}_{c'}\right)dS \tag{2}$$

where n denotes iterative times. $P.V.\int$ denotes the principal value of the integral and ∇G is the gradient of the free space Green's function. Based on the irradiation relationship between face elements, the multiple reflections of the electromagnetic wave can be simulated by the iterative calculation of Eq.(2). The forward-backward methodology is combined with relaxation factor w ($0 < w \le 1$) to accelerate the convergence and reduce the chance of divergence of the iterative solution [5]. According to experience, for the general cavity w is 0.8～0.9, and for the complicated cavity w is 0.6～0.7 [6]. The w is 0.8 during the calculation of current investigation.

4. Equivalent Edge Currents Method

EEC is a general method to calculate the edge diffraction field. With the method, the edge diffracted part of the scattered far field can be expressed by the equivalent electric and magnetic edge currents $\vec{I}(\vec{r}')$ and $\vec{M}(\vec{r}')$ as follows [7]:

$$\vec{E}^{d} = -jk\int_{c}[ZI(\vec{r}')\hat{s}\times(\hat{s}\times\hat{t}) + M(\vec{r}')(\hat{s}\times\hat{t})]G(\vec{r}',\vec{r})dl \tag{3}$$

$$\hat{s} = \frac{\vec{s}}{s} = \frac{\vec{r}-\vec{r}'}{\left|\vec{r}-\vec{r}'\right|}, \quad G(\vec{r}',\vec{r}) = \frac{e^{-jks}}{4\pi s}$$

where k is the wave number of incident electromagnetic wave; Z is the impedance of the surrounding medium; $\vec{r}$, $\vec{r}'$ are the position vector of the observation point and a certain point on the edge C respectively; dl is the increment of the arc-length l along the edge C. $\hat{s}$, s are the unit vector and the distance from a certain point on the edge C to the observation point respectively. $G(\vec{r}',\vec{r})$ is the three-dimensional Green's function; $\vec{I}(\vec{r}') = I(\vec{r}')\hat{t}, \vec{M}(\vec{r}') = M(\vec{r}')\hat{t}$ are the equivalent electric and magnetic edge currents respectively. The components of the edge diffracted part, I^f and M^f, are shown in Eq. (4) and Eq. (5) [8]. The calculation of I^f and M^f can be explained by a canonical wedge problem.

The geometry of the problem is depicted in Fig.7 [9]. The dashed lines are the projections of the directions of incidence and observation on the *xy*-plane. The point *O* is chosen as the origin. The *x* axis is directed along the normal to the edge lying on the "upper" face of the edge, and the *y* axis coincides with the external normal to this face. The *z* axis is directed along the edge, so as to form a right-hand system. $\hat{s}$ and $\hat{s}'$ are the directions of observation and incidence. The angles between the $\hat{s}$ and $\hat{s}'$ directions and the edge are β and β'. The angle between the "upper" face and the edge-fixed plane of incidence containing the vectors $\hat{s}'$ and $\hat{z}$ is ϕ'. The corresponding angle for the edge-fixed plane of observation is ϕ.

$$\begin{aligned} I^f = \frac{-2j}{kZ\sin^2\beta}\{&\frac{\sin\phi U(\pi-\phi)}{\cos\phi+\mu_1} + \frac{(1/N)\sin(\phi/N)}{\cos[(\pi-\alpha_1)/N]-\cos(\phi/N)} + \frac{\sin(N\pi-\phi)U(\pi+\phi-N\pi)}{\cos(N\pi-\phi)+\mu_2} + \\ &\frac{(1/N)\sin[N\pi-\phi)/N]}{\cos[(\pi-\alpha_2)/N]-\cos[(N\pi-\phi)/N]}\}\hat{z}\bullet\vec{E}_i + \{\frac{2j\sin[(\pi-\alpha_1)/N]}{Nk\sin\beta\sin\alpha_1}\bullet \\ &\frac{\mu_1\cot\beta' - \cot\beta\cos\phi}{\cos(\phi/N)-\cos[(\pi-\alpha_1)/N]} - \frac{2j\sin[(\pi-\alpha_2)/N]}{Nk\sin\beta\sin\alpha_2}\bullet \\ &\frac{\mu_2\cot\beta' - \cot\beta\cos(N\pi-\phi)}{\cos[(N\pi-\phi)/N]-\cos[(\pi-\alpha_2)/N]}\}\hat{z}\bullet\vec{H}_i \end{aligned} \tag{4}$$

$$M^f = \frac{2jZ\sin\phi}{k\sin^2\beta}\left\{\frac{U(\pi-\phi)}{\cos\phi+\mu_1} - \frac{(1/N)\sin[\pi-\alpha_1)/N]\csc\alpha_1}{\cos(\phi/N)-\cos[\pi-\alpha_1)/N]}\right\}\hat{z}\bullet\vec{H}_i + \frac{2jZ\sin(N\pi-\phi)}{k\sin^2\beta}$$
$$\left\{\frac{U(\pi+\phi-N\pi)}{\cos(N\pi-\phi)+\mu_2} - \frac{(1/N)\sin[\pi-\alpha_2)/N]\csc\alpha_2}{\cos((N\pi-\phi)/N)-\cos[\pi-\alpha_2)/N]}\right\}\hat{z}\bullet\vec{H}_i \tag{5}$$

$$\left.\begin{aligned}\cos\alpha_1 = \mu_1 = \cos\phi - 2\cot^2\beta\\ \cos\alpha_2 = \mu_2 = \cos(N\pi-\phi) - 2\cot^2\beta\end{aligned}\right\} \tag{6}$$

$$U(x) = \begin{cases}0, x \le 0\\ 1, x > 0\end{cases} \tag{7}$$

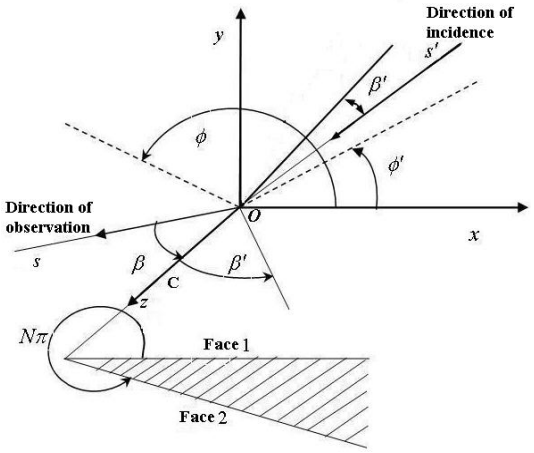

Fig.7 Wedge scattering geometry

5. Irradiation Relationship Judgment Based on Ray-Tracing

The irradiation relationship between face elements has to be judged before the induction current is calculated with the IPO. The ray-tracing method is applied in the present investigation to judge the irradiation relationship. The process is as following.

1) Generate the mesh in the cavity field. The boundary face elements of the mesh are used for IPO and the volume elements are used for ray-tracing to judge the irradiation relationship between face elements. Equivalent surface currents are evaluated on the inner walls of the cavity, so IPO has nothing to do with the cavity interior volume mesh. Therefore, the coarse volume meshes can be generated to increase the efficiency. The mesh of the cavity is shown in Fig.8.

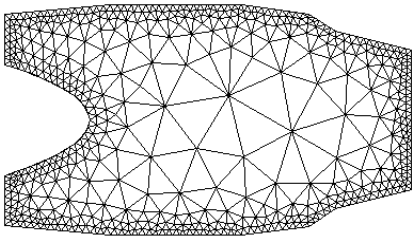

Fig.8 Sketch of the coarse volume mesh

2) For face elements A and B, if they can irradiate each other, the following conditions must be satisfied.

$$\vec{r}_{21}\bullet\vec{n}_1 > 0 \text{ and } \vec{r}_{21}\bullet\vec{n}_2 < 0 \tag{8}$$

where $\vec{r}_{21}$ denotes the vector from the center point of B to A. $\vec{n}_1$ and $\vec{n}_2$ are unit normal vector of A

and B respectively.

If above conditions can not be satisfied, the irradiation relationship between A and B does not exist, otherwise the following step should be performed sequentially.

3) A radial is assumed to radiate from the element center of A to B. Then, search the volume cells in the direction of the radial one by one and find the boundary face elements of the volume cells intersected with the radial. If any one of the boundary elements is opaque, the irradiation relationship between A and B dose not exist, as radial 1 shown in Fig.9. Otherwise, the irradiation relationship exists, as radial 2 in Fig.9.

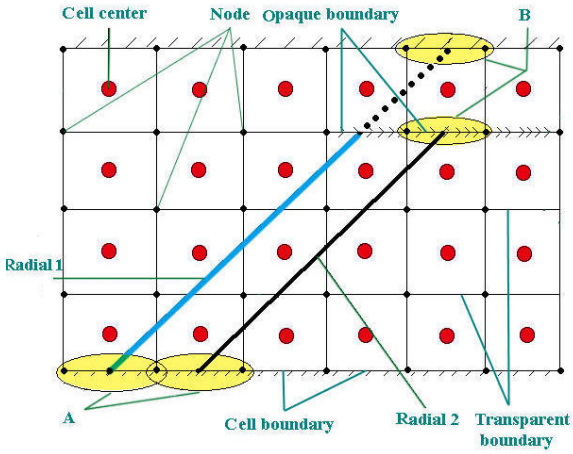

Fig.9 Illustration of ray-tracing

6. Validation of the Program

To validate the program, RCS of a cylindrical Open-ended cavity is calculated [10].The cavity axis is coincident with x axis of the coordinates, and the open direction is positive x. The frequency f of incident wave is 10 GHz. The cavity length L and diameter D are 10λ and 6λ respectively, where λ is the wavelength. Fig.10 and Fig.11 are numerical calculation results, where RCS ($\theta\theta$) and RCS ($\varphi\varphi$) denote the mono-static RCS in the horizontal and vertical polarization respectively.

As shown in Fig.10 and Fig.11, present calculation results agree with the dates of ref.10 within the range of calculation angles. Therefore, the program developed is reliable and accurate.

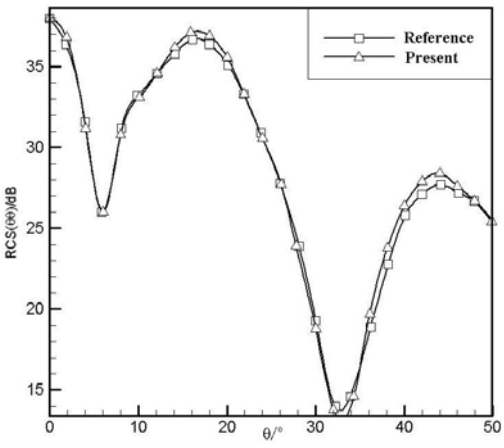

Fig.10 Horizontal polarization

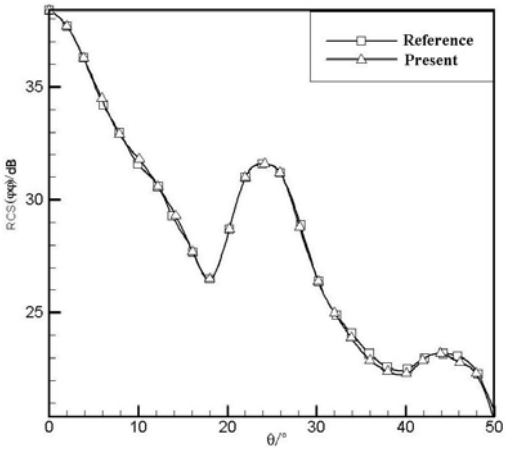

Fig.11 Vertical polarization

7. Presentation of Result

The definition of incident direction is shown in Fig.12, where θ is the space angle between

incident direction and positive x, and φ is the angle from positive y to the projection of incident direction at yOz.

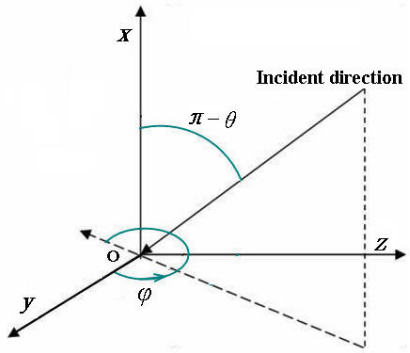

Fig.12 Definition of the incident direction

The nozzle axis is coincident with x axis, and the outlet direction is positive x. Fig.13 and Fig.14 show the cavity scattering RCS of the three nozzles under horizontal and vertical polarization respectively, where φ=0°, θ=0°～40°.

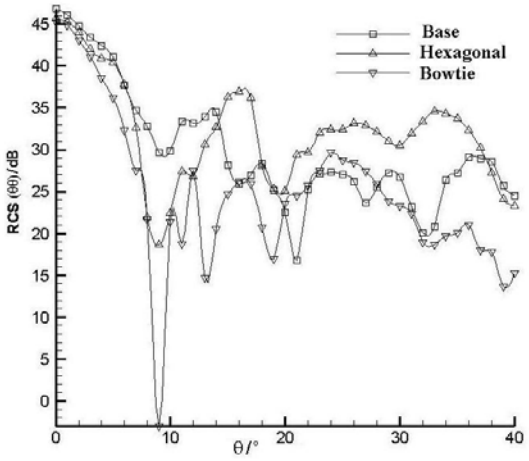

Fig.13 Horizontal polarization

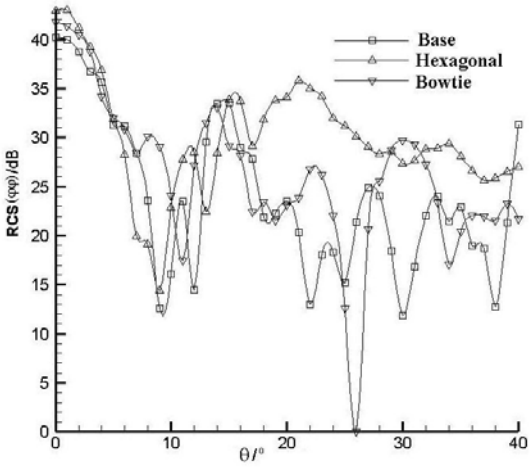

Fig.14 Vertical polarization

As shown in the figures, within the range of the azimuth angles, the RCS of three SCFN under two polarization conditions are obviously different. Within the wide range of azimuth angles, the RCS of bowtie SCFN is much less than the RCS of others. Specially, taking horizontal polarization for

example, as shown in Fig.13, the RCS of bowtie SCFN is less than the RCS of the others in most azimuth angles, such as $0°\leq\theta\leq19°$ and $29°\leq\theta\leq40°$. Furthermore, when the azimuth angle θ is about 0^{o}, the RCS of the three nozzles reaches the maximum at the same time. Obviously, the bowtie SCFN has the minimum RCS, -3dB and 0dB, under the two polarizations when the azimuth angle θ is 9° and 26° respectively. So considering from the aspect of the cavity scattering, the bowtie SCFN is better in RCS characteristics.

The induced current density on the detectable area at a certain azimuth angle can reflect the RCS at this angle indirectly. Taking horizontal polarization for example, Fig.15 and Fig.16 show the induced current density distribution of the three nozzles at the azimuth angles of 0° and 9° respectively. The figures also explain the reason why the minimum RCS is reached by the bowtie SCFN among the three SCFN when the azimuth angle is 9°. By comparing Fig.15 and Fig. 16, it is evident that the induced current density on the detectable area at the azimuth angle of 0° is larger than the induced current density at the azimuth angle of 9°. Since the inlet of the nozzle is simplified as a plane, and when the azimuth angle is 0°, most of the incident electromagnetic wave is reflected directly to form a strong echo. So, the induced current density is very large and the RCS of three nozzles at the azimuth angle of 0° reaches the maximum at the same time. Because the throat area of the three SCFN is equal to each other, the detectable area at the bottom of the nozzle cavities keeps identical. Therefore, the RCS of three SCFN at the azimuth angle of 0° is close to each other. When the azimuth angle is 9°, the incident electromagnetic wave reflects many times between the inner surfaces in the nozzle, and a little of them reflects back to the incidence direction. So the induced current density in this direction is very small and the RCS of three nozzles becomes lower relative to 0°azimuth angle. As shown in Fig. 16, the detectable area at the bottom of the bowtie SCFN is the least, so the induced current intensity is also the smallest. As a result, the RCS of the bowtie SCFN reaches the minimum at 9°azimuth angle.

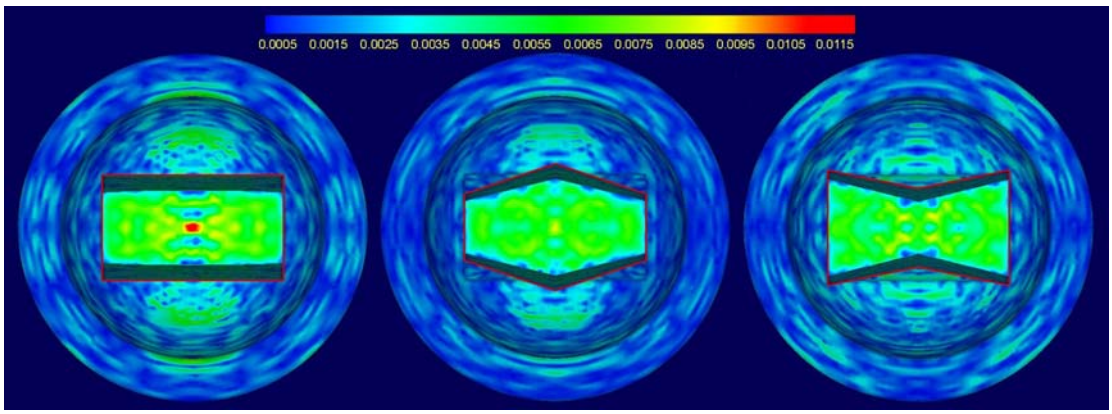

Fig. 15 Distribution of the induced current density (A/m) of the cavities at the azimuth angle of 0°

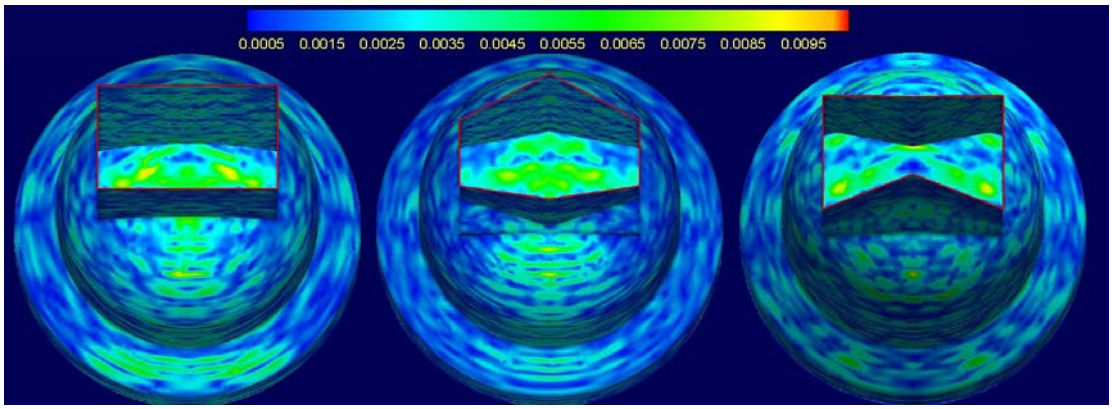

Fig. 16 Distribution of the induced current density (A/m) of the cavities at the azimuth angle of 9°

Fig. 17 and Fig. 18 show the edge diffraction RCS under the two polarizations respectively. As shown in the figures, the RCS of the hexagonal and bowtie nozzles are close to each other and much less than the RCS of the baseline one obviously. Under the condition of vertical polarization, the average edge diffraction RCS of the baseline nozzle is about 15dB within the range of the azimuth angles, but the average RCS of the other two nozzles is about -18dB, in other words, 33dB less than that of the baseline nozzle. Under the condition of horizontal polarization, the average edge diffraction RCS of the baseline nozzle is about 20dB more than that of the other two nozzles. Therefore, the edge diffraction RCS of hexagonal and bowtie SCFN can be decreased significantly.

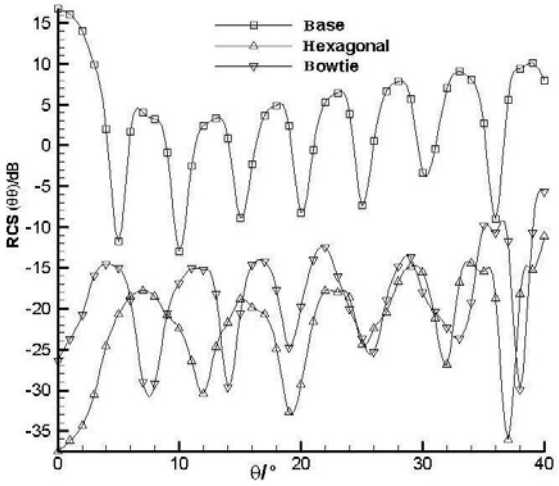

Fig.17 Horizontal polarization

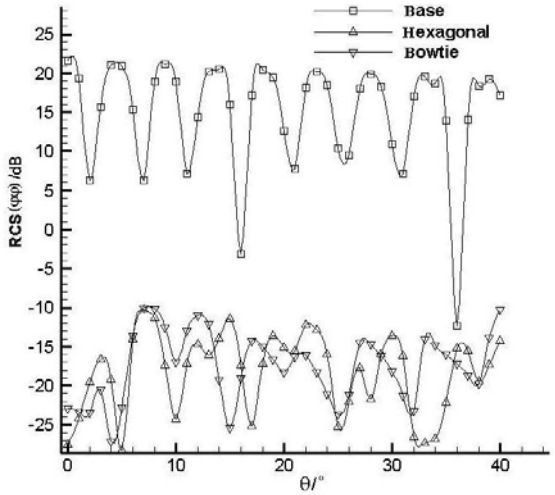

Fig.18 Vertical polarization

Within the range of the azimuth angles, the direction of the incident electric field may be parallel to the trailing edge of certain parts of the baseline SCFN, so the stronger current can be induced, and the edge diffraction RCS is large, according to the theory about the electromagnetic field. On the contrary, the hexagonal and bowtie SCFN with non-rectangular divergent duct can avoid the above situation, so the edge diffraction RCS can be decreased.

8. Conclusions

1) Combining IPO with EEC, a program is developed to calculate radar scattering characteristics

for the nozzle, and the results show that the program is reliable.

2) Edge diffraction RCS of the hexagonal and bowtie SCFN is less than RCS of the baseline SCFN. Non-rectangular divergent duct can decrease RCS greatly.

3) SCFN with bowtie divergent duct has the best radar stealth performance.

4) The current investigation adopts high-frequency asymptotic methods to calculate the RCS of the nozzle cavity. The inlet of the nozzle is simplified as a plane, so the electromagnetic scattering characteristics of the complex structures, such as the turbine, can't be calculated actually. The coupled algorithm of high-frequency and low-frequency will be developed at the follow-up works to calculate the RCS of the complex nozzle.

References

[1] Berrier B L, Taylor J G. Internal performance of two nozzles utilizing gimbal concepts for thrust vectoring. NASA /TP-2991, 1990.

[2] Taylor J G. Internal performance of a hybrid axisymmetric/nonaxisymmetric convergent-divergent nozzle. NASA TM-4230, 1991.

[3] David J W. Static Thrust and vectoring performance of a spherical convergent flap nozzle with a nonrectangular divergent duct. NASA/TP-1998-206912, 1998.

[4] Fernando O B, Jose L R , Burkholder R J. An iterative physical optics approach for analyzing the electromagnetic scattering by large open-ended cavities. IEEE Trans. Antennas Propagat.1995; 43(4):356-361.

[5] Burkholder R J, Lundin T. Forward-backward iterative physical optics algorithm for computing the RCS of Open-Ended cavities. IEEE Trans. Antennas Propagat.2005; 53(5):793-799.

[6] Yan Y B,Ge D B,Nie X C,et al. An improved IPO method applied to the analysis of EM scattering from a large Open-Ended cavity. Journal of Microwaves 2001; 17(1). [in Chinese]

[7] Che J, Tang S. RCS analysis of hypersonic cruise vehicle. Journal of Astronautic 2007; 28(1): 227-232. [in Chinese]

[8] Arie M. Elimination of infinities in equivalent edge currents, Part I: Fringe Current components. IEEE Trans. Antennas Propagat.1986; 34(7):912-918.

[9] Arie M. Equivalent edge currents for arbitrary aspects of observation. IEEE Trans. Antennas Propagat.1984; 32(3):252-258.

[10] Gu C Q, Shu Y Z, Xu J P. A subdomains splicing technique for IPO approach. Acta Electronica Sinica 2001; 29(3):420-422. [in Chinese]